Article

Digital Control Method and Performance Analysis of the Double-Compound Axial Piston Pump

Zhiyuan Sun, Qingliang Zeng,* Lirong Wan, and Jinying Jiang

Cite This: *ACS Omega* 2023, 8, 28592−28607

Read Online

ACCESS | 　📊 Metrics & More | 　📰 Article Recommendations

ABSTRACT: The flow control range of the double-compound axial piston pump with the traditional mechanical-hydraulic feedback servo control is limited and the accuracy is poor. Accordingly, this paper proposes a digital control scheme and its control strategy using a linear stepper motor direct drive servo valve for the precise control and double pumps cooperation of the double-compound axial piston pump. A numerical model of the digital control double-compound axial piston pump is established, and the validity of the model is verified by experimental tests. The performance advantages of the digital control method relative to the mechanical-hydraulic feedback servo control method are analyzed, as is the performance of the control strategy for double pumps. The results show that the digital control method can achieve a wider range of flow control than the traditional mechanical-hydraulic feedback servo control method and avoid the torque impact on the prime mover caused by the active control. The combination of the flow control and the power control including four control modes can meet the performance requirements of the double-compound axial piston pump. The highest priority is given to the energy-saving control, which can reduce the displacement of the main pump in the nonworking state to reduce the additional power loss. The study provides a basis for the accurate matching and optimization of power to load and flow to operating speed of the double-compound axial piston pump.
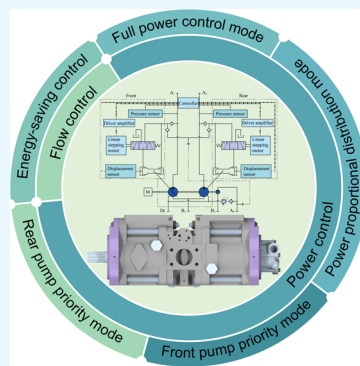
1. INTRODUCTION

A hydraulic system is widely used in engineering machinery, transportation, aerospace, and other industrial fields because of its high power density, flexibility, and high stiffness.[1−3] The hydraulic system is mainly divided into the pump-controlled hydraulic system and the valve-controlled hydraulic system. The pump-controlled hydraulic system is usually used in high-power scenarios, and its power loss is smaller than that of the valve-controlled hydraulic system.[4−6] The axial piston pump in the high-power pump-controlled hydraulic system is not only the main power source of the hydraulic system but also undertakes the responsibility of flow control.[7,8] To give full play to the advantages of the pump-controlled hydraulic system, it is an important development direction of the hydraulic variable pump to develop various variable control methods of the variable pump and effectively control pressure, flow, and power.[9,10] At the same time, with the development of digital hydraulic technology, the variable control mode of the variable pump has begun to develop in the direction of digitization, intelligence, and networking. The digital controller is used to improve the control performance of the hydraulic variable pump, to better match with the load, achieve the effect of saving energy, realize more functions and higher performance, and improve the competitiveness of the hydraulic transmission system.[11,12]

Recently, international participants have conducted plenty of theoretical, experimental, and simulation work on the digital control of hydraulic power systems. Heikkila et al.[13] proposed a displacement control method for the digital hydraulic power management system and analyzed the open-loop position tracking responses and the accuracy of steady-state velocity tracking with different loads. Spanu et al.[14] used a stepper motor to drive the reversing valve to form a high-precision closed-loop valve-controlled hydraulic pump system. The analysis results showed that this is a method to improve the efficiency of the hydraulic pump and system. Heitzig et al.[15] analyzed a digital pump consisting of several parallel constant pumps and several switching valves, which proved that the digital pump has more advantages in energy-saving than the traditional pump control system under partial load conditions of the multiactuator systems. Song et al.[16] designed a new load-sensing digital hydraulic system using pressure compensation technology and frequency conversion hydraulic technology. The system could adjust the oil supply pressure and the oil supply flow in real-time according to the change of the load pressure and the load flow, minimizing the throttling loss and
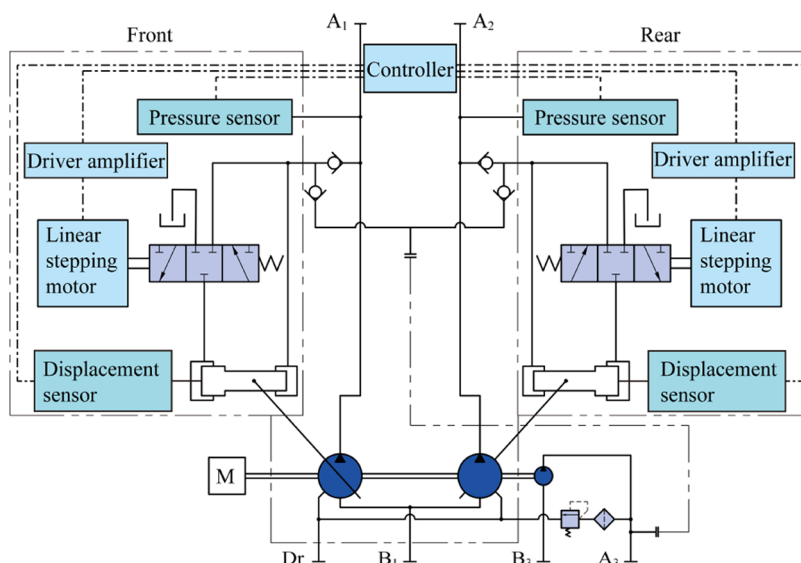
Figure 1. Digital control scheme for the DCAPP.

the overflow loss, and improving the system efficiency. Wang et al.[17] put forward a hydrostatic transmission system for the loader composed of the digital pump and the digital motor. Discrete variable control was used to realize stepwise automatic transmission, which can make the engine run stably in the economic area, thus reducing fuel consumption and improving the working efficiency of the whole machine. Gong et al.[18] proposed a real-time control strategy based on parameter rules for a new electro-hydraulic energy-saving system integrating recovery and regeneration devices and applied the system to 23 ton hydraulic excavators. The test showed that 17.6% of energy savings were achieved. Mitov et al.[19,20] developed an embedded control system for variable displacement axial piston pump based on the electro-hydraulic proportional valve, and then proposed an $H\infty$ algorithm for the displacement control of the axial piston pump to ensure the robustness of the closed-loop system in the presence of significant load disturbances.

Due to the advantages of tight structure, high working pressure, high power density, high volumetric efficiency, and easy variable realization, the double-compound axial piston pump (DCAPP) is often used as the main power source of high-pressure, high-speed, and high-power hydraulic systems.[21,22] Two axial piston pumps are installed symmetrically, sharing an intermediate of oil supply and discharge to form a series of shafts.[23] The DCAPP with traditional mechanical-hydraulic feedback servo control is equipped with two variable controllers to control the front and rear pumps, which can realize a common oil supply and separate oil supply for one or more working devices. At present, scholars have conducted extensive research on the realization and control methods of digital pumps, digital valves, and digital hydraulic systems. However, there are few studies on the digital control strategy and method of the DCAPP with special configuration. Consequently, in this study, a digital control scheme and its control strategy for the precise control and collaboration of the DCAPP are proposed. The numerical model of the digital control DCAPP is established, and the performance advantages of the digital control method relative to the mechanical-hydraulic feedback servo control method are analyzed. The performance of the control strategy for the DCAPP is analyzed,

which provides theoretical support and a study foundation for the accurate matching and optimization of power to load and flow to the working speed of the DCAPP.

2. NUMERICAL MODEL AND CONTROL METHOD OF THE DIGITAL CONTROL DOUBLE-COMPOUND AXIAL PISTON PUMP

2.1. Digital Control Scheme. The physical structure of the DCAPP and the mechanical-hydraulic feedback servo control system has been described and analyzed in detail in a previous study.[23] To improve the control accuracy and automatic control level of the DCAPP, the study proposes a digital control scheme based on the linear stepping motor for the DCAPP based on the traditional mechanical-hydraulic feedback servo control of the DCAPP, as shown in Figure 1. The scheme is mainly composed of a front pump, a rear pump, a front pump regulator, a rear pump regulator, a controller, and an intermediate. The front pump and the rear pump, as well as the front pump regulator and the rear pump regulator, have the same structure and are installed symmetrically relative to the intermediate. The regulator is mainly composed of a pressure sensor, a displacement sensor, a drive amplifier, and a linear stepping motor.

In order to avoid the additional pressure loss caused by the configuration of the flowmeter in the system and reduce the cost, a displacement sensor is installed at the actuator piston, and the position of the actuator piston is detected to be converted into the inclination angle of the swash plate. Then, the theoretical output flow is calculated by using Formulas 1 and 2. The method is used to monitor the output flow equivalently and form the feedback of the target flow.

$$q = k_p n x_{ap} \tag{1}$$

$$k_p = \frac{\pi d_p^2 D z}{4 L_{sp}} \tag{2}$$

where k_p is the displacement gradient of the piston pump, n is the shaft speed of the piston pump, x_{ap} is the displacement of the actuator piston, d_p is the piston diameter, D is the diameter

of the piston pitch circle, z is the number of pistons, and L_{sp} is the acting force arm of the actuator piston to the swash plate.

The outlet pressure and the displacement of the actuator piston of the front and rear pump circuits are transmitted to the controller. The controller uses Formula 1 to convert the calculation of the displacement of the actuator piston into the output flow value of the piston pump and then calculates the output power values of the front and rear pumps. By comparing with the preset flow curve, the controller determines whether the output flow should be increased or decreased, then sends a PWM control signal, enabling signal and direction signal to the drive amplifier of the linear stepping motor, to control the action of the linear stepping motor and realize the opening and closing of the servo valve port.

The flow control process of the DCAPP is illustrated using the front pump as an example, as shown in Figure 1. The controller sends the signals to the linear stepper motor when the output flow of the front pump is less than the expected value or the output power is less than the expected value. The servo valve spool moves to the left under the drag of the linear stepping motor and the right function position starts to work, at which point the servo valve controls the large cavity of the actuator piston to drain oil. The small cavity of the actuator piston is always connected to the high-pressure working oil circuit of the front pump, so the hydraulic force at the end of the small cavity is higher than that at the end of the large cavity. And then the actuator piston moves to the left, dragging the inclination angle of the swash plate to increase. Therefore, the displacement of the front pump increases, the output flow increases, and the output power increases. On the contrary, when the output flow of the front pump is greater than the expected value or the output power is greater than the expected value, the linear stepping motor drives the servo valve spool to move to the right, and the servo valve controls the working oil circuit to connect the large cavity of the actuator piston. The hydraulic force of the end of the large cavity is greater than that of the end of the small cavity, the actuator piston moves to the right. Then, the swash plate angle decreases and the displacement of the front pump decreases. Therefore, the output flow decreases and the output power decreases.

2.2. Numerical Model. According to the digital control scheme of the DCAPP, the dynamic model of the pump body of the DCAPP is established first. Each piston cavity is modeled as a capacitive volume model, and its pressure is obtained by integrating the expression of the time derivative.[24,25] The instantaneous pressure in the piston cavity is expressed as

$$\frac{dp_{p,i}}{dt} = \frac{E}{V_{p,i}}\left(-Q_{pin,i} - Q_{pout,i} - Q_{lpcb,i} - Q_{lssp,i} - \frac{dV_{p,i}}{dt}\right)$$

(3)

where $p_{p,i}$ is the pressure of the piston cavity, E is the bulk modulus of hydraulic oil, $Q_{pin,i}$ is the inlet flow of the piston cavity, $Q_{pout,i}$ is the outlet flow of the piston cavity, $Q_{lpcb,i}$ is the leakage flow between the piston and the cylinder block, $Q_{lssp,i}$ is the leakage flow between the slipper and the swash plate, and $V_{p,i}$ is the volume of the piston cavity.

The piston performs compound motion with the shaft, and the volume of the piston cavity is given as

$$V_{p,i} = V_0 + d_p^2 \pi R[\tan \beta_0 + \tan \beta \sin(\omega t)]/4$$

(4)

where V_0 is the structure dead volume of the piston cavity, R is the radius of the piston pitch circle, β is the inclination angle of the swash plate, β_0 is the initial inclination angle of the swash plate, and ω is the rotational speed of the shaft.

The structure between the piston cavity and the port plate is regarded as a thin-walled orifice. Therefore, the flow between the piston cavity and the inlet and outlet of the port plate is turbulent. And the flow rates $Q_{pout,i}$ and $Q_{pin,i}$ through the simple throttle orifice are expressed as[24]

$$\begin{cases} Q_{pin,i} = C_d A_{pin,i}\sqrt{\dfrac{2|p_{p,i} - p_s|}{\rho}}\, \text{sign}\ (p_{p,i} - p_s) \\ Q_{pout,i} = C_d A_{pout,i}\sqrt{\dfrac{2|p_{p,i} - p_d|}{\rho}}\, \text{sign}(p_{p,i} - p_d) \end{cases}$$

(5)

where C_d is the flow coefficient, $A_{pin,i}$ is the flow area between the ith piston cavity and the inlet silencing groove, $A_{pout,i}$ is the flow area between the ith piston cavity and the outlet silencing groove, p_s is the inlet pressure of the pump, p_d is the outlet pressure of the pump, and ρ is the density of hydraulic oil.

The leakage of the kinematic pair of an axial piston pump is mainly composed of three parts: the leakage of the slipper–swash plate pair, the leakage of the piston–cylinder block pair, and the leakage of the port plate–cylinder block pair.[26] Since the leakage of the pilot pump and control valve does not affect the output performance of the main pump, and the control valve leakage is relatively small, this additional flow leakage is not considered. To accurately calculate the outlet flow rate, numerical calculations are required for the leakage of the slipper–swash plate pair, the piston–cylinder block pair, and the port plate–cylinder block pair. The total leakage flow is expressed as

$$Q_l = \sum_{i=1}^{N} Q_{lpcb,i} - \sum_{i=1}^{N} Q_{lssp,i} - Q_{lppc}$$

(6)

where Q_{lppc} is the leakage flow between the port plate and the cylinder block.

The leakage flow of the piston–cylinder block pair is given as

$$Q_{lpcb,i} = \frac{\pi d_p h_p}{4\mu_{p,i} l_{pc,i}}(p_{p,i} - p_c)\left(\frac{h_p^2}{24} + \frac{e_p^2}{4}\right) + \frac{\pi d_p h_p}{2}u_{p,i}$$

(7)

where h_p is the diameter clearance between the piston and the piston cavity, $\mu_{p,i}$ is the dynamic viscosity of the piston–cylinder block pair clearance, $l_{pc,i}$ is the contact length between the piston and the piston cavity, p_c is the pressure of the leakage cavity, e_p is the eccentricity between the piston and the piston cavity, and $u_{p,i}$ is the Couette effect of the piston velocity on the leakage flow.

The leakage flow of the slipper–swash plate pair is given as[27]

$$Q_{lssp,i} = \frac{\pi(p_{p,i} - p_c)h_{ssp}^3 d_{tp}^4}{\mu_{p,i}[6d_{tp}^4 \ln(r_{spo}/r_{spi}) + 128h_{ssp}^3 l_{tp}]}$$

(8)

where h_{ssp} is the clearance between the slipper and the swash plate, d_{tp} is the diameter of the piston damping orifice, r_{spo} is the outer radius of the slipper, r_{spi} is the inner radius of the slipper, and l_{tp} is the length of the piston damping orifice.

The leakage of the port plate—cylinder block pair is divided into two parts, the leakage Q_{lcpi} between the cylinder block and the port plate inlet and the leakage Q_{lcpo} between the cylinder block and the port plate outlet. The leakage flow is given as[28]

$$
\begin{aligned}
Q_{lppc} &= Q_{lcpi} + Q_{lcpo} \\
&= -\frac{\theta_{in} h_{ppc}^3 (p_s - p_c)}{12\mu}\left[\frac{1}{\ln\ (r_{ext1}/r_{ext2})} - \frac{1}{\ln(r_{int1}/r_{int2})}\right] \\
&\quad - \frac{\theta_{out} h_{ppc}^3 (p_d - p_c)}{12\mu}\left[\frac{1}{\ln\ (r_{ext1}/r_{ext2})}\right. \\
&\quad \left. - \frac{1}{\ln\ (r_{int1}/r_{int2})}\right]
\end{aligned}
$$
(9)

where h_{ppc} is the clearance between the cylinder block and the port plate, θ_{in} is the angle range of the silencing groove at the inlet of the port plate, θ_{out} is the angle range of the silencing groove at the outlet of the port plate, r_{int1} is the outer radius of the internal port plate, r_{int2} is the inner radius of the internal port plate, r_{ext1} is the inner radius of the external port plate, and r_{ext2} is the outer radius of the external port plate, and μ is the dynamic viscosity.

The inlet and outlet flow rates of the pump are the sum of the inlet and outlet flow rates of all piston cavities through the port plate. The phase angle of each piston is considered

$$
Q_{in} = \sum_{i=1}^{N} Q_{pin,i(\varphi i)} - Q_{lpbi}
$$
(10)

$$
Q_{out} = \sum_{i=1}^{N} Q_{pout,i(\varphi i)} - Q_{lpbo}
$$
(11)

Given the inlet and outlet operating conditions of the pump, the shaft power input, and the operating state of the swash plate, the model can calculate the pressure of the piston cavity by Formula 3, and then use the equations to calculate the flow rates of piston cavities. Finally, the inlet and outlet flow rates and the leakage flow rates are calculated using Formulas 6, 10, and 11.

The oil pressure in each piston cavity acts on the bottom surface of the piston, and the equivalent force $F_{p,i}$ is applied to the middle of the bottom surface of the piston and is perpendicular to it (i.e., along the z-axis). The viscous friction $F_{vlpc,i}$ caused by the leakage of the piston—cylinder block pair is also applied to the piston along the z-axis.

$$
\begin{cases}
F_{p,i} = p_{p,i} \dfrac{d_p^2}{4} \\
F_{vlpc,i} = 2\pi(d_p - h_p)\left(\dfrac{p_{p,i} - p_c}{8}h_p - \dfrac{1}{h_p}\mu_{p,i} l_{pc,i} u_{p,i}\right)
\end{cases}
$$
(12)

Therefore, the composite force acting on each piston is given as

$$
F_{pt,i} = F_{p,i} + F_{vlpc,i}
$$
(13)

The viscous friction generated by the rotation of each slipper on the swash plate is given as

$$
F_{vls,i} = \frac{\pi \mu_{p,i} \omega R}{h_{ssp}}(r_{spo}^2 - r_{spi}^2)
$$
(14)

The torque applied to the swash plate by the piston is given as

$$
T_{sp} = \sum_{i=1}^{N} y_{p,i}(F_{ptz,i} + F_{vlsz,i}) - \sum_{i=1}^{N} z_{p,i}(F_{pty,i} + F_{vlsy,i})
$$
(15)

where $y_{p,i}$ is the force arm of the composite force along the z-axis in the y-direction; $z_{p,i}$ is the force arm of the composite force along the y-axis in the z-direction; $F_{ptz,i}$ and $F_{pty,i}$ are the projections of the composite force $F_{pt,i}$ on the z-axis and y-axis, respectively; and $F_{vlsz,i}$ and $F_{vlsy,i}$ are the projections of the composite force $F_{vls,i}$ on the z-axis and y-axis, respectively.

The viscous friction torque between the port plate and the cylinder block is given as

$$
T_{vlpp} = \frac{\mu\omega}{4h_{ssp}}[(r_{int\ 1}^4 - r_{int\ 2}^4) + (r_{ext1}^4 - r_{ext2}^4)](\theta_{in} + \theta_{out})
$$
(16)

Therefore, the shaft torque of the piston pump is given as

$$
T_{sf} = \sum_{i=1}^{N} x_{p,i}(F_{pty,i} + F_{vlsz,i}) - \sum_{i=1}^{N} y_{p,i} F_{vlsx.i} + T_{vlpp}
$$
(17)

The variable control model is established in accordance with the variable swash plate control system. Based on the pressure signal and the control algorithm, the controller calculates the frequency, quantity, and direction of the pulse under the logical condition, and outputs the pulse signal. And the linear stepping motor drives the displacement of the servo valve spool.

$$
x_{sv} = \frac{l\theta_s N}{2\pi}
$$
(18)

where l is the lead, θ_s is the step angle, and N is the number of pulses.

The linearized flow equation of the servo valve is expressed as

$$
q_{sv} = k_q x_{sv} - k_c p_{ap}
$$
(19)

$$
k_q = C_d w_{sv}\sqrt{2(p_d - p_{ap})/\rho}
$$
(20)

$$
k_c = C_d w_{sv} x_{sv}\sqrt{2(p_d - p_{ap})/\rho}\,/2(p_d - p_{ap})
$$
(21)

where p_{ap} is the pressure of the large cavity of the actuator piston, k_q is the flow gain, k_c is the flow—pressure coefficient, and w_{sv} is the flow area of the servo valve.

The flow continuity equation of the control cavity of the actuator piston is expressed as

$$
q_{sv} = A_d \frac{dx_{ap}}{d_t} - C_l(p_d - p_{ap}) + \frac{V_{ap}}{E}\frac{dp_{ap}}{dt}
$$
(22)

where A_d is the action area of the large cavity of the actuator piston, C_l is the internal leakage coefficient of the actuator piston, and V_{ap} is the volume of the large cavity of the actuator piston.

The kinetic equation of the actuator piston is expressed as

$$
A_d p_{ap} - A_x p_d = m_{ap}\frac{d^2 x_{ap}}{dt^2} + c_{ap}\frac{dx_{ap}}{dt} + F_{sp}
$$
(23)

where A_x is the action area of the small cavity of the actuator piston, m_{ap} is the mass of the actuator piston, c_{ap} is the viscous damping coefficient of the actuator piston, and F_{sp} is the force of the swash plate on the actuator piston.

The kinetic equation of the swash plate is expressed as

$$F_{sp}L_{sp} - T_{sp} = J_{sp}\frac{d^2\beta}{dt^2} + c_{sp}\frac{d\beta}{dt} \tag{24}$$

where J_{sp} is the rotational inertia of the swash plate and c_{sp} is the damping coefficient of the swash plate.

A large amount of air dissolved in the fluid is released, which is called aeration, when the pressure in the hydraulic fluid is lower than the saturation pressure. When the fluid pressure decreases to a certain value, it causes the fluid to evaporate and produce a large amount of vapor, which is called cavitation. This happens when the pressure reaches saturated vapor pressure. The chemical properties of the hydraulic fluid are not pure, so it does not occur under a single pressure, but within a certain pressure range. The characteristic modeling of hydraulic fluid is described in IMAGING,[29] taking into account the aeration and cavitation phenomena and the compressibility, which is used to calculate the density and viscosity of the hydraulic fluid.

2.3. Control Strategy of Double Pumps. A control strategy combining flow control, power control, and energy-saving control is proposed in accordance with the working requirements of the DCAPP, as shown in Figure 2. The flow
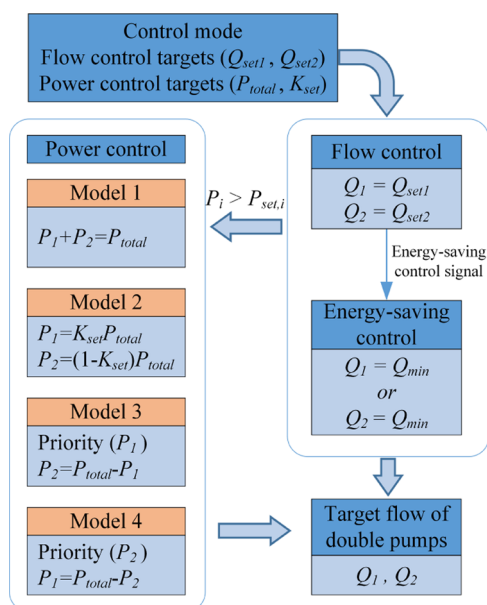

Figure 2. Flowchart of the control strategy.

control is active flow control, i.e., the output flow of the two main pumps is actively controlled according to the requirements of the execution unit within the power-limiting conditions. The flow control is automatically converted into

the power control when the power of a single pump or double pumps touches a power-limiting wall, which is determined by the power control mode and its set parameters. The energy-saving control can be regarded as a special case of the flow control, i.e., when the execution unit is nonworking, the main pump runs at the minimum displacement and reduces the output flow, which can effectively reduce the energy loss. In the control strategy, the priority of energy-saving control is the highest.

The power control includes four control modes, full power control mode (Mode 1): The output flow of a main pump is not only controlled by its power but also by the power of another main pump. This mode can not only make full use of the output power of the prime mover, but also allow the other main pump to use all of the remaining power when the power of one of the pumps is reduced, and ensure that the phenomenon of overload work does not occur. At the same time, the output flow of the two main pumps is the same, and the action of the execution unit (e.g., hydraulic cylinder) is consistent. The power proportional distribution mode (Mode 2): The two main pumps distribute the total power in a certain proportion, and the power distribution of different execution units is adjusted independently to realize the independent control of the two main pumps and to ensure that no overload occurs in the two main pumps. The front pump priority mode (Mode 3): In the power distribution of the two main pumps, the priority of the front pump is higher, i.e., the output power of the front pump is guaranteed first, and the rear pump can output at the lowest displacement. The rear pump priority mode (Mode 4): Similar to the front pump priority mode, the rear pump has a higher priority in the power distribution between the two main pumps. The power distribution of the two main pumps is the rear pump priority, i.e., the output power of the rear pump is preferentially guaranteed, and the front pump can output at the lowest displacement.

3. NUMERICAL SIMULATION MODEL AND MAIN PUMP PERFORMANCE TEST VERIFICATION

According to the numerical model of the DCAPP, the equations are compiled based on AMESim, and the submodel of the axial piston pump body is established. The variable control submodels of the front pump and rear pump and the controller submodel are established in accordance with the variable control model and the digital control method of the DCAPP. Then, the numerical simulation model of the digital control DCAPP is established. The specifications of the main pump and the properties of the hydraulic oil are shown in Tables 1 and 2.[23] The model is composed of the axial piston pump body submodel, the controller submodel, the variable control submodel, the simulated loading submodel, and the simulated data collection submodel, as shown in Figure 3.

The experimental object of the pump body of the DCAPP is used to verify the accuracy and reliability of the numerical simulation model of the pump body of the DCAPP. Figures 4 and 5 show the schematic diagram and the test bench of the performance test system for the DCAPP. The front pump, the

Table 1. Specifications of the DCAPP

displacement (mL/r)	flow (L/min)		pressure (bar)		speed (rpm)	
	max.	min.	rated	peak	rated	max.
$2 \times 115 \pm 2$	$2 \times 207 \pm 3$	$2 \times 30 \pm 3$	343	400	1800	2700

Table 2. Properties of the Hydraulic Oil

parameter	value	parameter	value
density (kg/m³)	876	gas content	0.1%
bulk modulus (MPa)	1700	saturation pressure (MPa)	7.1×10^{-2}
dynamic viscosity (Pa·s)	5.1×10^{-2}	high saturated vapor pressure (MPa)	3.3×10^{-3}
temperature (°C)	40−60	low saturated vapor pressure (MPa)	1.8×10^{-3}

rear pump, and the pilot pump of the tested pump are driven coaxially by the prime mover and loaded by the electro-hydraulic proportional valve. The pilot pump and the pilot pressure unit provide the pilot pressure for the test system. The oil recovery unit is applied to filter and recover the external leakage oil of the test system. A variety of sensors are installed on the test bench, as shown in Figure 4, which are used to measure the shaft speed, shaft torque, outlet flow, outlet pressure, leakage flow, etc. The technical characteristics of the sensors are shown in Table 3.[23] The test bench allows the tested pump to adjust the shaft speed, load pressure, pilot pressure, etc. To reduce the impact of the test system on the surrounding environment and protect the safety of staff, the entire test system hardware is enclosed in an isolation box, as shown in Figure 5a.

In order to validate the numerical simulation model, the experimental test and the numerical simulation are carried out under the same working conditions. To fully test the performance of the pump body of the DCAPP, the rear pump is operated unloaded at minimum displacement. The load pressure of 0−300 bar is applied to the front pump, and the shaft speed is 1800 rpm.

Figure 6 shows the experimental results and numerical simulation results of the performance of the DCAPP. In the test results, there is some fluctuation in the output flow of the front pump, which is caused by the flow pulsation, as shown in Figure 6a. In the numerical simulation, the instantaneous output flow is averaged as the output flow value, so the fluctuation is not visible. On the overall trend, the output flow of the front pump test decreases with the increase of the load pressure and basically presents a linear relationship. The flow loss is caused by the flow leakage of the piston pump, hence the leakage flow of the piston pump is basically positively linearly correlated with the load pressure. In addition, the numerical simulation results of the output flow show the same trend as the experimental results, and the experimental results fluctuate around the numerical simulation results. Therefore, the numerical simulation of the output power of the DCAPP is highly accurate, as shown in Figure 6b. Comparing the shaft torque versus overall efficiency curves obtained from the experimental test and the numerical simulation, the experimental test and numerical simulation results show the same trend and are in good agreement, as shown in Figure 6c,d. However, there are still some deviations with a maximum deviation of 23.44 N m for the shaft torque and 0.08 for the overall efficiency, which is acceptable.

Comparing the results of the experimental test and numerical simulation of the pump body performance, the results of the experimental test and numerical simulation show the same trend and are in good agreement, and the error is within the allowable range. Hence, the numerical simulation method is accurate and reliable for the performance analysis of the pump body of the DCAPP, and the reliability and accuracy of the numerical simulation model of the pump body of the DCAPP are high. Therefore, the numerical simulation model
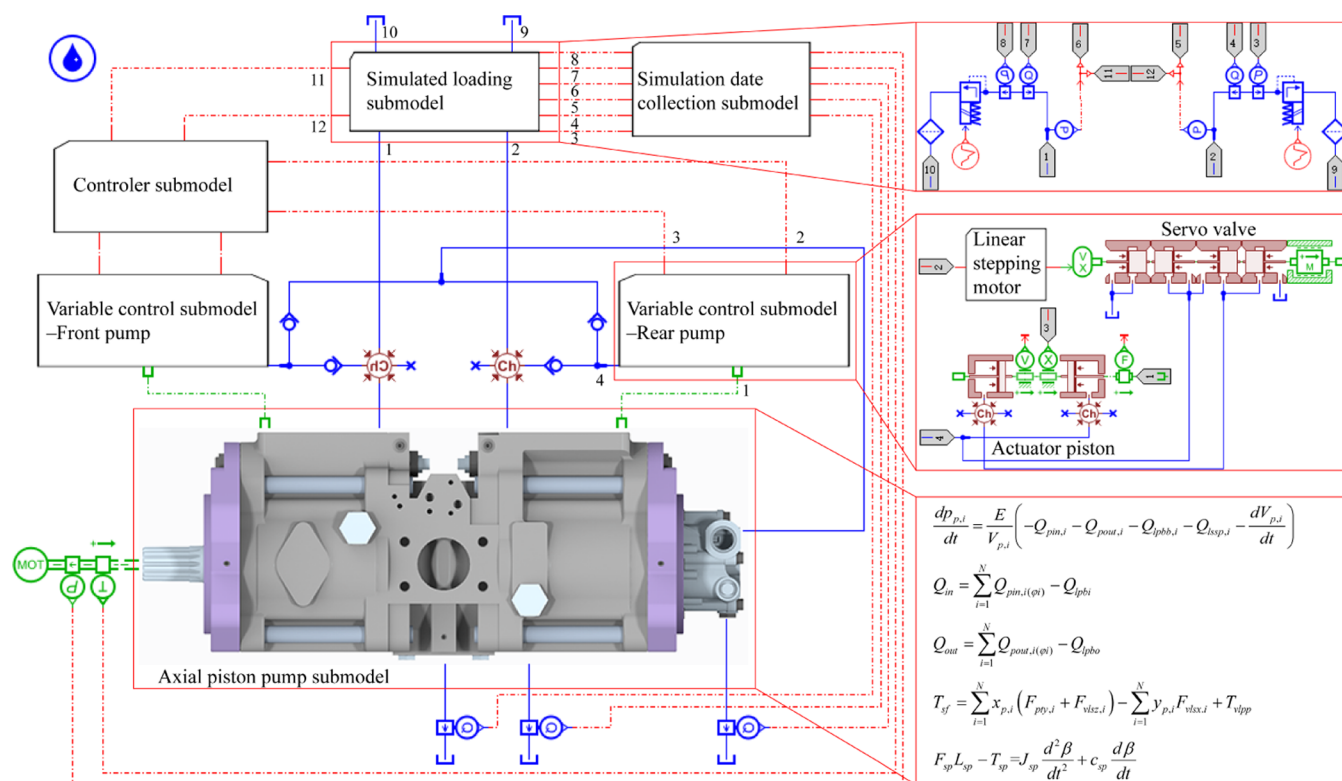

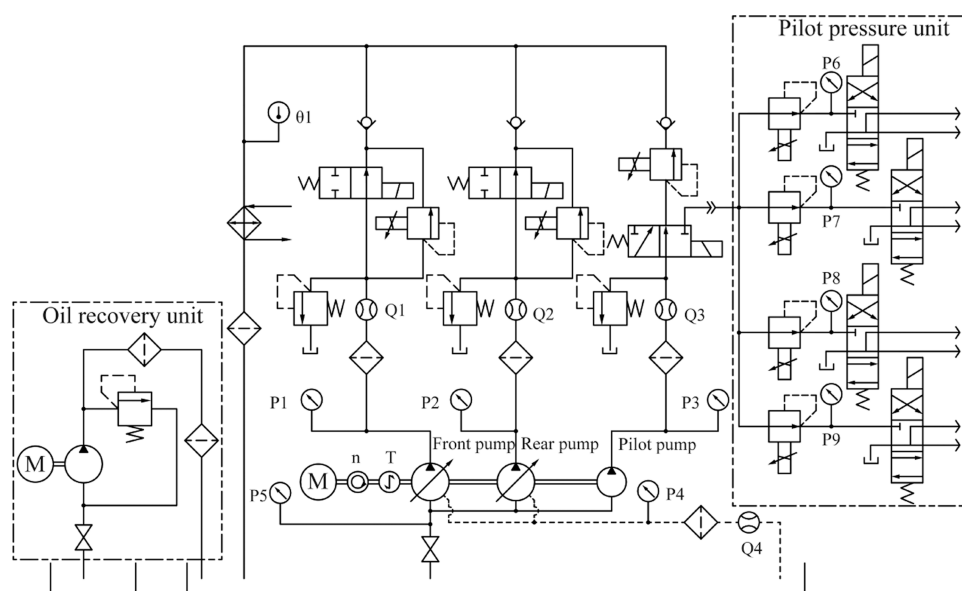**Figure 3.** Numerical simulation model of the digital control DCAPP.

Figure 4. Schematic diagram of the performance test system for the DCAPP.
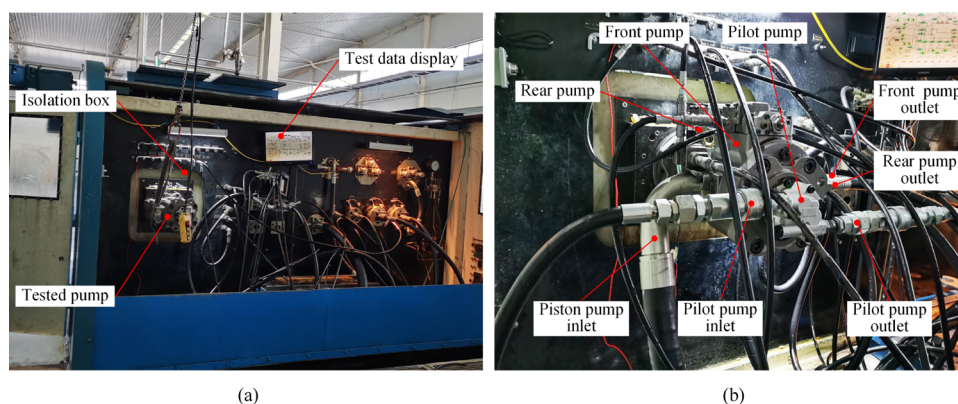

Figure 5. Performance test system for the DCAPP: (a) test bench; (b) tested pump.

Table 3. Technical Characteristics of Measuring Sensors

tag	sensor	range	accuracy
n, T	torque speed	0–4000 r/min, 0–2000 N·m	0.2% F·S
Q1, Q2	flow	1.5–525 L/min	0.3% F·S
Q3, Q4	flow	0.03–40 L/min	0.3% F·S
θ_1	temperature	−40 to 350 °C	±1.0 °C
P1, P2	pressure	0–450 bar	0.125% F·S
P3, P6, P7, P8, P9	pressure	0–60 bar	0.125% F·S
P4	pressure	0–10 bar	0.125% F·S
P5	pressure	−1 to +5 bar	0.125% F·S

of the digital control DCAPP is accurate and effective for its performance analysis.

4. RESULTS AND DISCUSSION

4.1. Advantage Analysis of Digital Control Method for the Double-Compound Axial Piston Pump. The original mechanical-hydraulic feedback servo control method mainly adopts a cross-power control mode, and its control mainly relies on the cooperation of the power control valve and the dual power control springs. The detailed control principle and characteristics have been described in a previous study.[23] Under this control method, the main pump flow can only be

adjusted on the constant power control curve, and the flow control curves under different set output power can be selected by controlling the pilot pressure. As a result, its control range of flow is limited and the accuracy is low.

The performance of the DCAPP with the digital control method is analyzed and compared with the mechanical-hydraulic feedback servo control method in the previous study. The numerical simulation of the DCAPP with two control methods is carried out under the same working conditions and setting conditions. Thus, the shaft speed is 1800 rpm, the output power is 107 kW, and the load pressure is 0–350 bar.
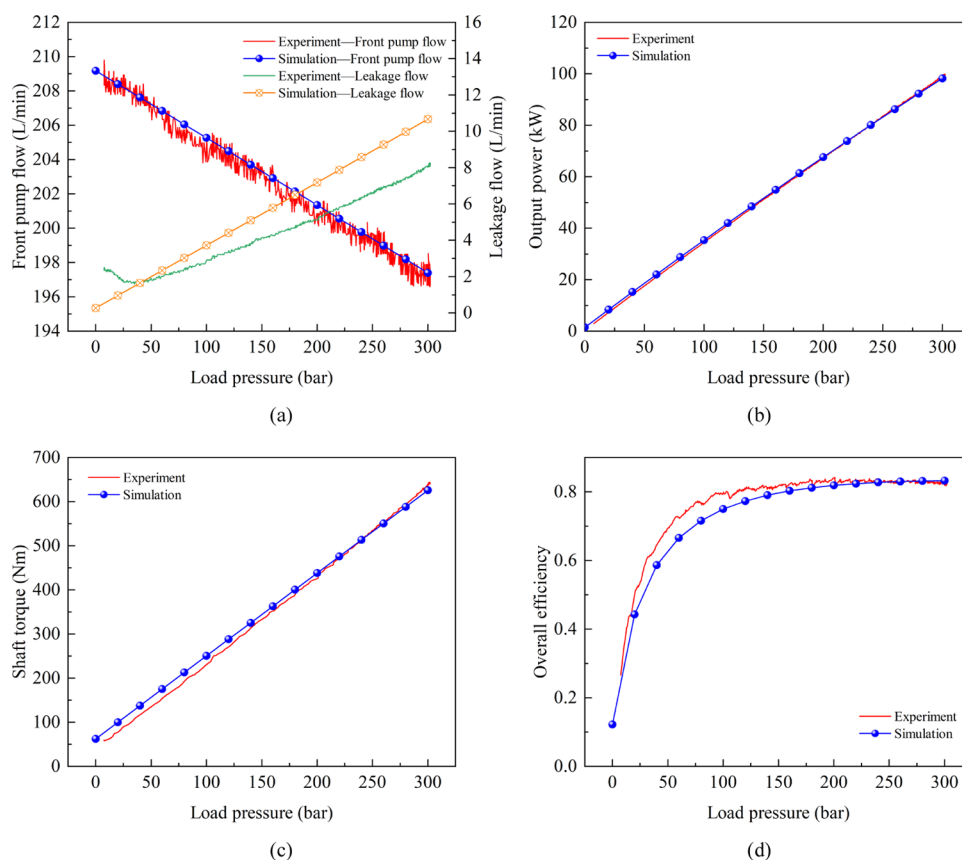
Figure 6. Comparison of experimental and numerical simulation results for the pump body performance: (a) flow; (b) output power; (c) shaft torque; (d) overall efficiency.
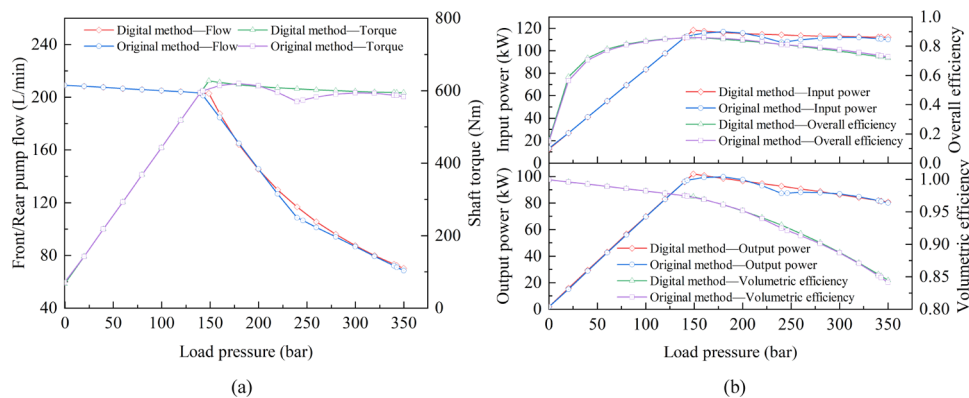

Figure 7. Performance comparison of the DCAPP with different control methods: (a) flow and shaft torque; (b) input power, output power, overall efficiency, and volumetric efficiency.

The performance comparison of the DCAPP with different control methods is shown in Figure 7. Compared with the original mechanical-hydraulic feedback servo control method, the power starting pressure of the DCAPP under the digital control method is larger. When the load pressure is less than the power starting pressure, the output flow of the two methods is the same. The constant power section of the flow curve of the mechanical-hydraulic control method is composed of two straight line segments, while the constant power section of the flow curve of the digital control method is a smooth curve, as shown in Figure 7a. The output power curve of the constant power section of the mechanical-hydraulic control method shows a double peak shape, but the output power

curve of the constant power section of the digital control method is basically linear. It can be seen that the output power stability of the digital control method is higher than that of the mechanical-hydraulic control method. Since the leakage flow increases with the increase of the load pressure, the output power of the constant power section decreases with the increase of the load pressure. Similar to the output power, the curves of the shaft torque and the input power in the constant power section of the mechanical-hydraulic control method show a double peak shape, while the curves of the shaft torque and the input power in the constant power section of the digital control method vary more smoothly, and the input power decreases slightly with an increase in the load pressure.
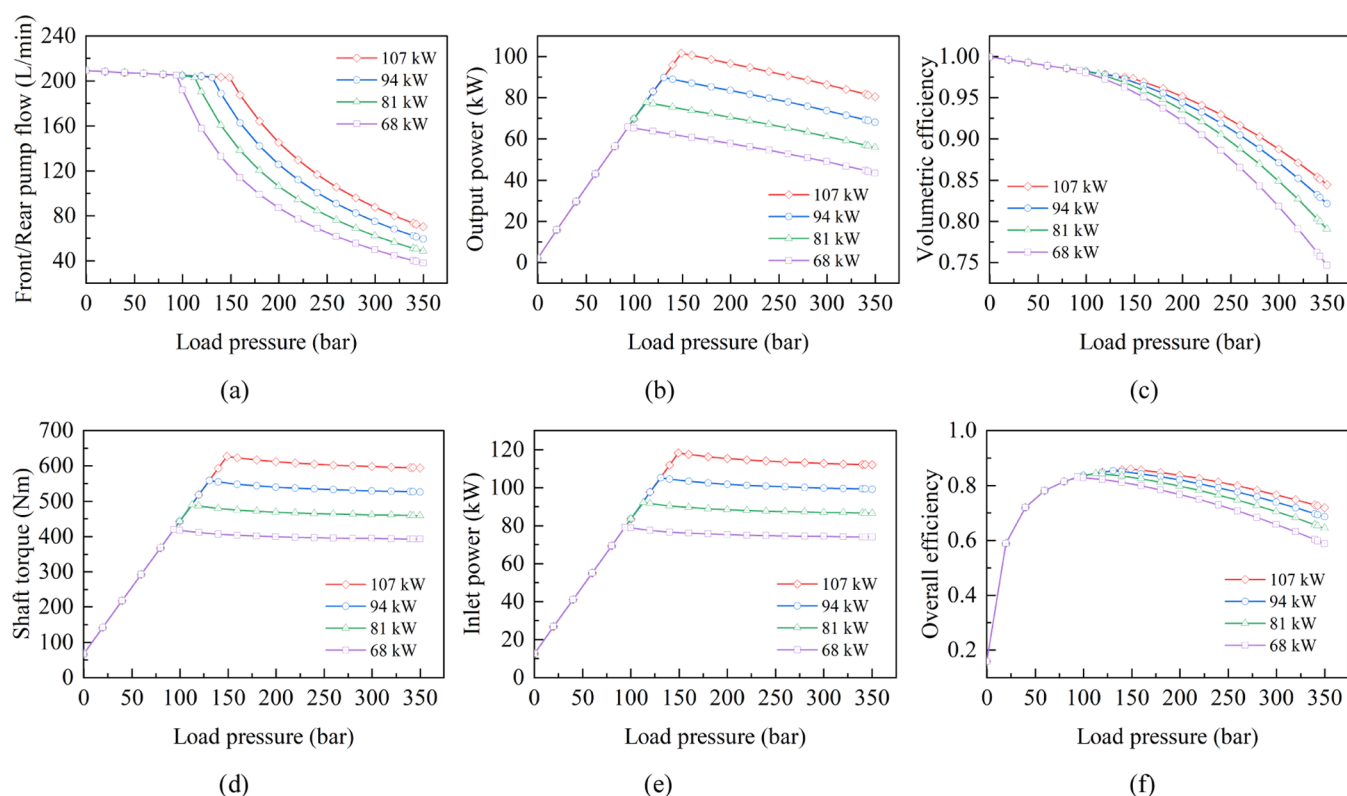
Figure 8. Performance of the piston pump in the full power control mode at different hydraulic output powers: (a) flow; (b) output power; (c) volumetric efficiency; (d) shaft torque; (e) input power; (f) overall efficiency.

The maximum output power of the DCAPP with the mechanical-hydraulic feedback servo control method is 99.73 kW, and the maximum input power is 116.89 kW. The maximum output power of the DCAPP with the digital control method is 101.78 kW, and the maximum input power is 118.24 kW. Therefore, the digital control method has a 2.1% advantage in the maximum output power for the same set power. The overall efficiency is the greatest around the power starting point, and the volumetric efficiency decreases with the increase of the load pressure. In the operating pressure range, the overall efficiency and volumetric efficiency of the DCAPP with the digital control method are essentially the same as those of the original method. There is a certain deviation between the maximum output power of the two methods and the set value, which is mainly caused by the flow leakage of the piston pump.

By comparison, the digital control method can fully meet the performance requirements of the DCAPP and can achieve a wider range of flow control. In addition, compared with the mechanical-hydraulic feedback servo control method, the input power and shaft torque are more stable in the constant power section, avoiding the torque impact caused by the active control on the prime mover. Therefore, the digital control method adopted is superior to the traditional mechanical-hydraulic feedback servo control method in terms of the output and input characteristics of the DCAPP.

4.2. Performance Analysis of the Control Strategy for the Double-Compound Axial Piston Pump. The control strategy of the DCAPP is mainly composed of flow control, power control including four control modes, and energy-saving control. The performance of the front and rear pumps with different control modes determines the overall performance of the DCAPP. Among them, the power control mainly includes the full power control mode, the power proportional control mode, the front pump priority control mode, and the rear pump priority control mode. The flow control and the power control are deeply combined, and the area below the power control curve is the flow control, i.e., the flow control is automatically converted to the power control when the power reaches the power threshold.

4.2.1. Full Power Control Mode. In the full power control mode, the shaft speed is 1800 rpm and the set hydraulic output power values are 107, 94, 81, and 68 kW, respectively. The front and rear pumps are the same load pressure, and the performance characteristics of the DCAPP in the full power control mode at different hydraulic output powers are analyzed.

Figure 8 shows the performance of the piston pump in the full power control mode at different hydraulic output powers. The outlet flow curve presents two linear sections, and the inflection point between the two flow curves is the power set pressure point, as shown in Figure 8a. As the set power decreases, the power setting point decreases. The first section of the flow curve is a constant flow section, and the flow in this section is the maximum output flow. The second section of the flow curve is a constant power section, which is approximately the first quadrant of the inverse proportional function curve, and the difference between the flow curve and the standard curve is mainly caused by the flow leakage. Due to the control strategy of the full power control mode, the output flow of the front and rear pumps is the same. It is clear that the output flow decreases with the decrease of the set power value under the same load in the constant power section.
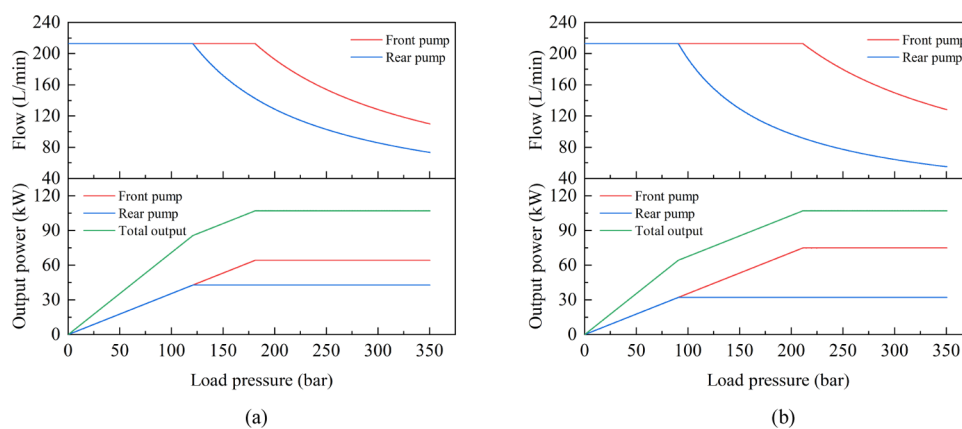
Figure 9. Control strategy objectives of the power proportional distribution control mode at different power distribution ratios: (a) 0.6; (b) 0.7.
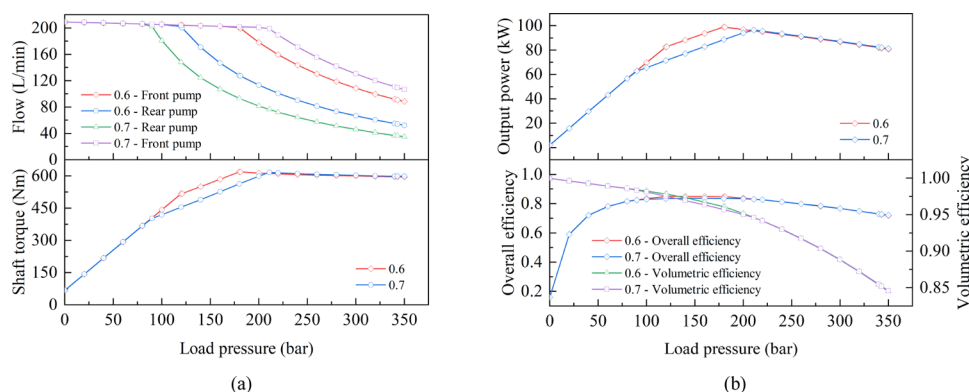

Figure 10. Performance of the piston pump in the power proportional distribution control mode at different power distribution ratios: (a) flow and shaft torque; (b) output power, overall efficiency, and volumetric efficiency.

Because the leakage flow is positively correlated with the load pressure, the output power is the largest at the power setting point, and the overall efficiency is the highest, as shown in Figure 8b,f. It is clear that the output power decreases with the decrease of the set power. The shaft torque of the piston pump is the largest at the power set pressure point. In the constant power section, the shaft torque decreases slightly with an increase in the load pressure, and the shaft torque decreases with the decrease of the set power. In addition, the input power of the piston pump shows the same trend as the shaft torque. In the constant flow section, the different set power values do not affect the performance of the piston pump. In the constant power section, the overall efficiency and volumetric efficiency decrease with a decrease in the set power.

4.2.2. Power Proportional Distribution Control Mode. In the power proportional distribution control mode, the shaft speed is 1800 rpm, the set hydraulic output power value is 107 kW, and the power distribution ratios are 0.6 and 0.7, respectively. The front and rear pumps are the same load pressure, and the performance characteristics of the piston pump in the power proportional distribution control mode at different power distribution ratios are analyzed.

Figure 9 shows the output targets of the control strategy of the piston pump controller in the power proportional distribution control mode at different power distribution ratios. In this control mode, the controller first distributes the total power of the piston pump to the front and rear pumps according to the power distribution ratio, at which point the control mode of the main pump is converted into constant

power control. It can be seen from Figure 9a that the front and rear pumps enter the constant power section after reaching the power set pressure point, respectively, and the output power values are following the pre-allocated ratio. The total output power of the piston pump is the superposition of the output power of the front and rear pumps, so the total output power curve has two inflection points, which are the power set pressure point of the rear pump and the front pump, respectively. Therefore, the front pup and rear pumps form an independent control and are not affected by each other. When the power distribution ratio is greater than 0.5, the distance between the power set pressure points of the front pump and the rear pump increases with the increase of the power distribution ratio. When the power distribution ratio is less than 0.5, the distance between the power set pressure points of the front pump and the rear pump increases with the decrease of the power distribution ratio. In principle, the power distribution ratio of the DCAPP can be set arbitrarily according to the demand, but it should be noted that the distribution power of the main pump is limited by the maximum power of the main pump.

Figure 10 shows the performance of the piston pump in the power proportional distribution control mode at different power distribution ratios. Pearson correlation coefficient is used to measure the linear correlation between the output values of the piston pump and the target values of the controller.
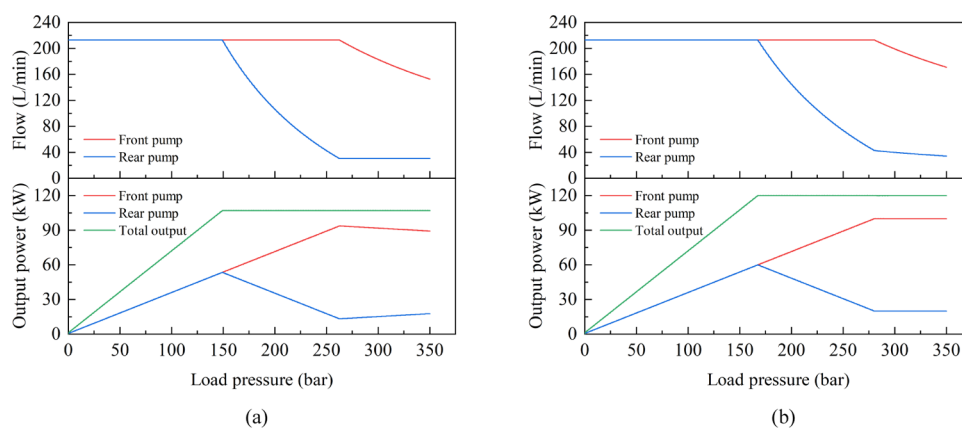
Figure 11. Control strategy objectives of the front pump priority control mode at different hydraulic output powers: (a) 107 kW; (b) 120 kW.
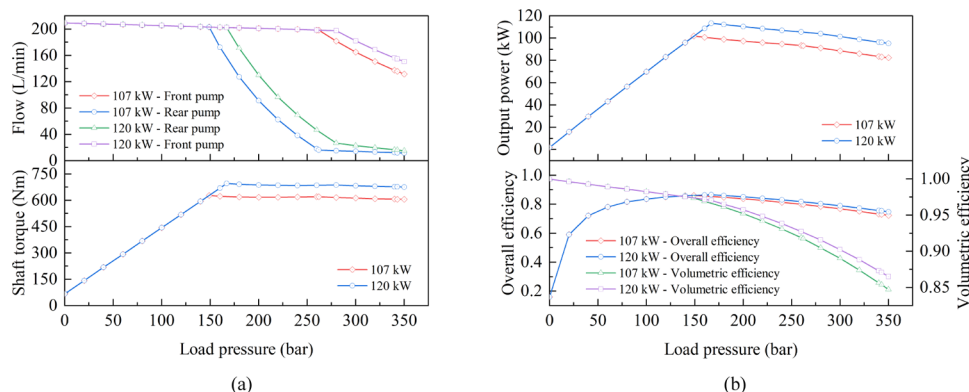

Figure 12. Performance of the piston pump in the front pump priority control mode at different hydraulic output powers: (a) flow and shaft torque; (b) output power, overall efficiency, and volumetric efficiency.

$$r_{XY} = \frac{\sum_{i=1}^{N}(X_i - \overline{X})(Y_i - \overline{Y})}{\sqrt{\sum_{i=1}^{N}(X_i - \overline{X})^2}\sqrt{\sum_{i=1}^{N}(Y_i - \overline{Y})^2}} \tag{25}$$

where X_i and Y_i are data points in the two sets of data.

Formula 25 is used to calculate the Pearson correlation coefficient between the output flow and output power of the piston pump and the target values of the controller in Figures 9 and 10. The correlation coefficient of the output flow is greater than 0.99, and the correlation coefficient of the output power is greater than 0.97. Therefore, the output flow and output power of the DCAPP show a strong linear correlation with the target values of the piston pump controller, and the difference between the output value and the target values is mainly caused by the flow leakage. The shaft torque of the piston pump presents a three-segment line, and the two inflection points between the three-segment lines are the power set pressure points of the front pump and the rear pump. In the section between the two inflection points, the shaft torque of the piston pump with a power distribution ratio of 0.6 is greater than that of the piston pump with a power distribution ratio of 0.7. However, in the other two sections, the power distribution ratio does not affect the shaft torque. The output power of the piston pump shows the same trend as the shaft torque. Similarly, in the section between the two inflection points, the overall efficiency and volumetric efficiency of the piston pump with a power distribution ratio of 0.6 are higher than those of the piston pump with a power distribution ratio of 0.7. However, in the other two sections, the overall

efficiency and volumetric efficiency at different power distribution ratios are the same.

4.2.3. Front Pump Priority Control Mode. In the front pump priority control mode, the shaft speed is 1800 rpm, and the set hydraulic output power values are 107 kW and 120 kW, respectively. The front and rear pumps are the same load pressure, and the performance characteristics of the piston pump in the front pump priority control mode at different hydraulic output powers are analyzed.

Figure 11 shows the output targets of the control strategy of the piston pump controller in the front pump priority control mode at different set powers. In this control mode, the output of the front pump is ensured by the controller preferentially, i.e., sufficient power is allocated to the front pump first. It can be seen from Figure 11a that there is a power set pressure point on the flow curve of the front pump, but there are two inflection points on the flow curve of the rear pump. The first is the power set pressure point for the rear pump, and the second corresponds to the power set pressure point for the front pump. At the power set pressure point of the rear pump, the total output power of the piston pump reaches the set power value. Due to the priority principle of the front pump, the output of the front pump is not affected, but the rear pump needs to reduce the power accordingly to ensure the operation of the front pump until it reaches the power set pressure point of the front pump. In the operating range after the power set pressure point of the front pump, the working state of the double pumps is affected by the set power value of the piston pump.
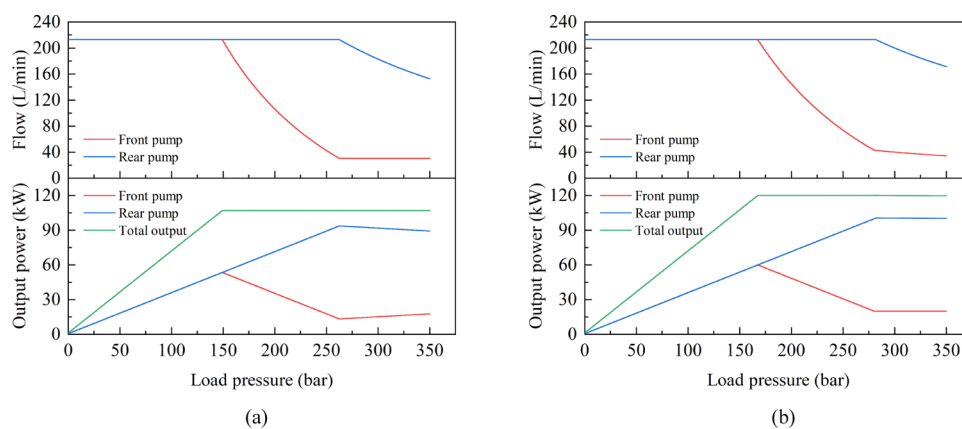
Figure 13. Control strategy objectives of the rear pump priority control mode in different hydraulic output power: (a) 107 kW; (b) 120 kW.
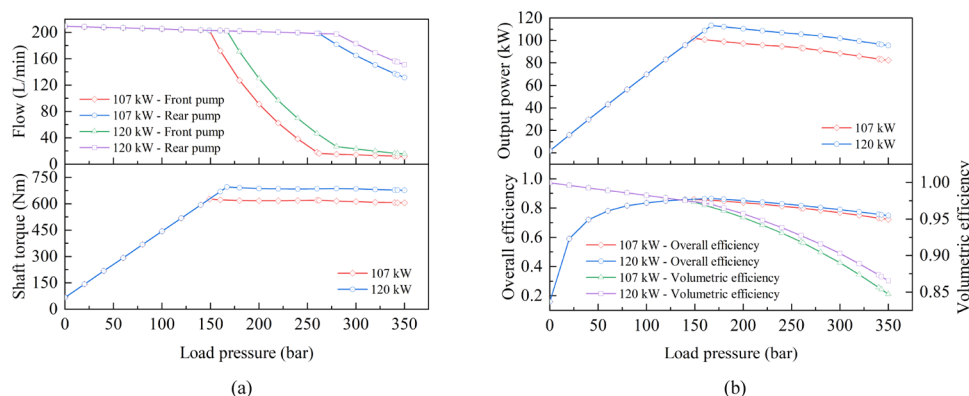

Figure 14. Performance of the piston pump in the rear pump priority control mode at different hydraulic output powers: (a) flow and shaft torque; (b) output power, overall efficiency, and volumetric efficiency.

As a set power of 107 kW, the output flow of the rear pump is reduced to the minimum output flow of the main pump when the power set pressure point of the front pump is reached so that the output power of the rear pump increases with the increase of the load pressure. The strategy of the front pump priority fails in this zone due to the limitation of the minimum flow rate of the rear pump, but the front pump still maintains a certain degree of priority. The increase in the output power of the rear pump leads to a decrease in the output power of the front pump, as shown in Figure 11a. Therefore, the power set pressure point of the front pump is affected by the minimum output flow of the rear pump at this point. As a set power of 120 kW, the output power of the front pump reaches the maximum output power of the main pump when the power set pressure point of the front pump is reached so that both the front and rear pumps are converted into independent constant power control, as shown in Figure 11b. Therefore, the power set pressure point of the front pump is affected by the maximum output power of the front pump.

Figure 12 shows the performance of the piston pump in the front pump priority control mode at different hydraulic output powers. Formula 25 is used to calculate the Pearson correlation coefficient between the output flow and output power of the piston pump and the target values of the controller in Figures 11 and 12. The correlation coefficient of the output flow is greater than 0.99, and the correlation coefficient of the output power is greater than 0.98. Therefore, in the front pump priority control mode, the output flow and output power of the DCAPP show a strong linear correlation with the target values

of the controller, and the difference between the output value and the target value is mainly caused by the flow leakage. The shaft torque of the piston pump presents two lines. The inflection point between the two lines is the power set pressure point of the rear pump, and the shaft torque at the power set pressure point is the largest. In the constant power section, the shaft torque decreases slightly with an increase in the load pressure, and the shaft torque increases with the increase of the set power. The input power of the piston pump shows the same trend as the shaft torque. In the constant flow section, different set power values do not affect the performance of the piston pump. In the constant power section, the overall efficiency and volumetric efficiency increase with an increase in the set power. In the strategy of front pump priority, the power of the front pump is simultaneously limited by the maximum power of the main pump.

4.2.4. Rear Pump Priority Control Mode. In the rear pump priority control mode, the shaft speed is 1800 rpm, and the set hydraulic output power values are 107 kW and 120 kW, respectively. The front and rear pumps are the same load pressure, and the performance characteristics of the piston pump in the rear pump priority control mode at different hydraulic output powers are analyzed.

Figure 13 shows the output objectives of the control strategy of the piston pump controller in the rear pump priority control mode at different hydraulic output powers. In contrast to the front pump priority control mode, the rear pump priority control mode gives the controller priority in ensuring the output of the rear pump, i.e., priority is given to allocating
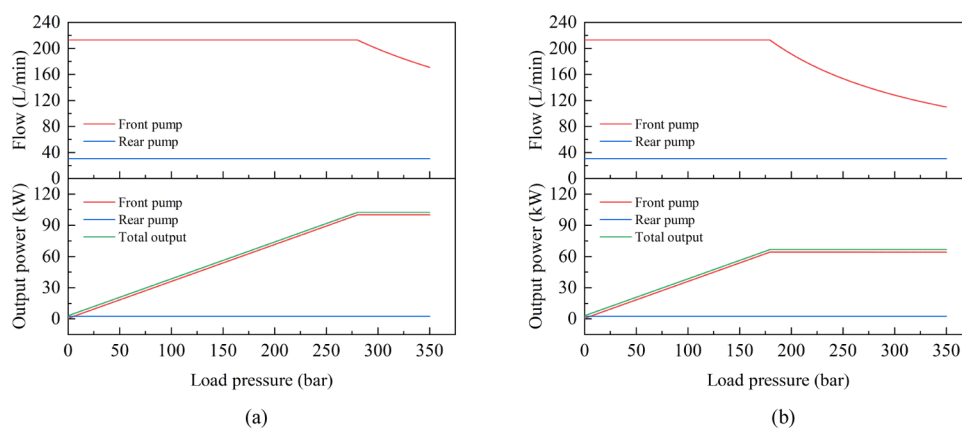
(a)   (b)

Figure 15. Control strategy objectives for the energy-saving control of the rear pump in the power control: (a) full power control mode; (b) power proportional distribution control mode.
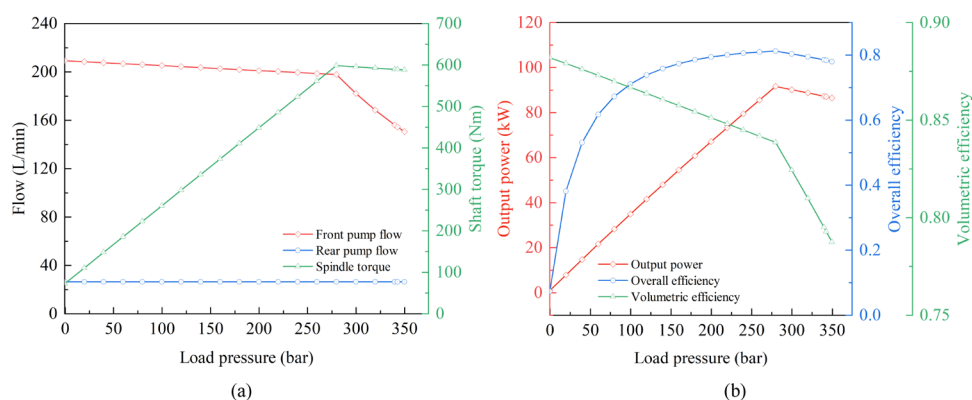

(a)   (b)

Figure 16. Performance of the piston pump with the rear pump energy-saving control in the full power control mode: (a) flow and shaft torque; (b) output power, overall efficiency, and volumetric efficiency.

sufficient power to the rear pump. There is a power set pressure point on the flow curve of the rear pump and two inflection points on the flow curve of the front pump, the first being the power set pressure point for the front pump and the second corresponding to the power set pressure point for the rear pump, as shown in Figure 13a. At the power set pressure point of the front pump, the total output power of the piston pump reaches the set power value. Due to the priority principle of the rear pump, the output of the rear pump is not affected, but the front pump needs to reduce the power accordingly to ensure the operation of the rear pump until it reaches the power set pressure point of the rear pump. The working state of the double pumps in the operating range after the power set pressure point of the rear pump is affected by the set power value of the piston pump.

Comparing the front pump priority control mode and the rear pump priority control mode under the two set power conditions, the control strategy objectives of the front pump in the rear pump priority control mode are the same as the control strategy objectives of the rear pump in the front pump priority control mode. Similarly, the control strategy objectives of the rear pump in the rear pump priority control mode are the same as the control strategy objectives of the front pump in the front pump priority control mode, as shown in Figures 11 and 13.

Figure 14 shows the performance of the piston pump in the rear pump priority control mode at different hydraulic output powers. Formula 25 is used to calculate the Pearson correlation

coefficient between the output flow and output power of the piston pump and the target values of the controller in Figures 13 and 14. The correlation coefficient of the output flow is greater than 0.99, and the correlation coefficient of the output power is greater than 0.97. Therefore, the output flow and output power of the DCAPP in the rear pump priority control mode also show a strong linear correlation with the target values of the controller. The performance of the shaft torque, input power, overall efficiency, and volumetric efficiency of the piston pump in the rear pump priority control mode is similar to that of the piston pump in the front pump priority control mode, i.e., the front pump and the rear pump exchange with each other. Similarly, in the strategy of rear pump priority, the power of the rear pump is also limited by the maximum power of the main pump.

4.2.5. Energy-Saving Control. The energy-saving control is carried out in the power control, and the independent energy-saving control is carried out for the rear pump of the piston pump in the full power control mode and the power proportional distribution mode, respectively. The load pressure of the nonworking rear pump is 48 bar, the shaft speed is 1800 rpm, the set hydraulic output power value is 107 kW, and the power distribution ratio in the power proportional distribution mode is 0.6.

Figure 15 shows the output targets of the control strategy for the energy-saving control of the rear pump in the full power control mode and power proportional distribution mode. In the control strategy for the DCAPP, the priority of energy-
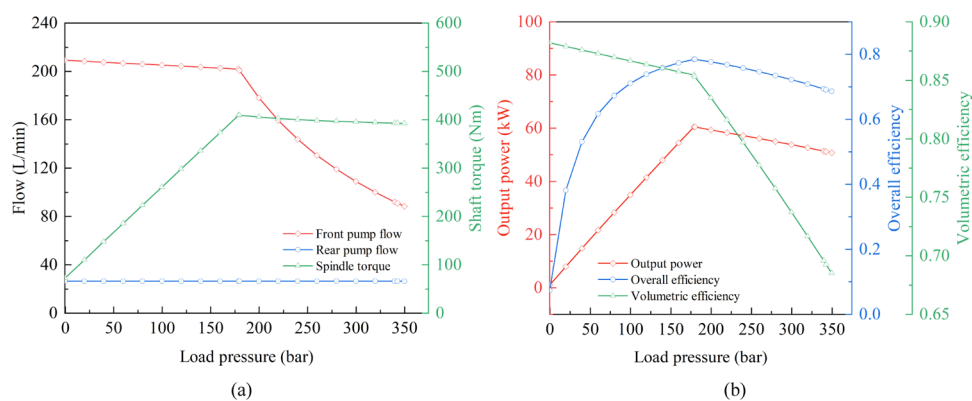
Figure 17. Performance of the piston pump with the rear pump energy-saving control in the power proportional distribution mode: (a) flow and shaft torque; (b) output power, overall efficiency, and volumetric efficiency.

saving control is the highest. The front and rear pumps of the piston pump can be independently energy-saving controlled, while the main pump with the non-energy-saving control works in the original control mode. With the energy-saving control of the rear pump, the rear pump operates at a minimum output flow so that the flow rate is reduced when the rear pump is in a nonworking state to reduce the additional power loss. In the full power control mode, with the energy-saving control of the rear pump, the front pump utilizes the remaining power but is limited by the maximum power of the single pump. In the power proportional distribution mode, with the energy-saving control of the rear pump, the front pump is not affected by the energy-saving control and still performs constant power control according to the pre-allocated power, as shown in Figure 15b.

Figures 16 and 17 show the performance of the piston pump with the energy-saving control of the rear pump in the full power control mode and the power proportional distribution mode, respectively. Formula 25 is used to calculate the Pearson correlation coefficient between the output flow and output power of the piston pump and the target values of the controller in Figures 14–16. The correlation coefficient of the output flow is greater than 0.98, and the correlation coefficient of the output power is greater than 0.98. Therefore, the output flow and output power of the DCAPP show a strong linear correlation with the target values of the piston pump controller. The difference between the output and target values is mainly caused by the flow leakage. The energy-saving control is performed on the rear pump of the piston pump in the full power control mode. The rear pump is nonworking and still consumes power, but the power consumption of the rear pump is less, as shown in Figures 15 and 16. The energy-saving control is performed on the rear pump of the piston pump in the power proportional distribution mode. The front pump is not affected by the energy-saving control, so the required power of the piston pump in this state is small, as shown in Figure 17. The overall efficiency and volumetric efficiency of the DCAPP with the energy-saving control are relatively low, but the additional power consumption caused by the nonworking pump is greatly reduced. In the constant power working section after the power set pressure point of the front pump, the volumetric efficiency is greatly affected by the load pressure, which is due to the decrease of the output flow of the working pump entering the constant power control state.

5. CONCLUSIONS

In this study, a digital control scheme and its control strategy of the DCAPP are proposed to realize the digital control of the DCAPP and improve the independent working and collaboration ability of the double pumps. The numerical model of the digital control DCAPP is established, and the accuracy and reliability of the pump body model are verified by experiments. The performance of the DCAPP in each control mode was verified and analyzed. The conclusions are as follows:

(1) A digital control scheme based on a linear stepping motor is proposed for the problems of the limited control range and double pump cooperation of the DCAPP under the traditional mechanical-hydraulic feedback servo control. According to the working requirements of the DCAPP, a control strategy combining flow control, power control including four control modes, and energy-saving control is proposed. The numerical simulation method used is verified to be accurate and reliable through the experiments. The numerical model of the DCAPP established can effectively analyze the performance of the DCAPP.

(2) Compared with the traditional mechanical-hydraulic feedback servo control method, the digital control method can fully meet the performance requirements of the DCAPP and achieve a wider range of flow control. And the input power and shaft torque of the constant power section is more stable, which avoids the torque impact on the prime mover caused by the active control. The digital control method adopted is superior in the output and input characteristics of the DCAPP.

(3) In the full power control mode, the output flow of the main pump is not only controlled by its power but also by the power of another main pump. This mode can not only make full use of the output power of the prime mover but also allow the other main pump to use all of the remaining power when the power of one pump is reduced and can ensure that there is no overload. In the power proportional distribution control mode, the controller first distributes the total power of the piston pump to the front and rear pumps, respectively, according to the power distribution ratio, and the control mode of the main pump is converted into the constant power control. In the front pump priority control mode, the output power of the front pump is guaranteed first, and the rear pump can output at the

lowest displacement. The rear pump priority control mode is the opposite.

(4) In the control strategy of the DCAPP, the priority of energy-saving control is the highest. The front and rear pumps of the piston pump can be independently energy-saving controlled, and the main pump with the non-energy-saving control works in the original control mode. With the energy-saving control of the nonworking pump, the nonworking pump works at the minimum displacement so that the nonworking pump is in the nonworking state to reduce the additional power loss.

The results of the study provide a digital control scheme and its control strategy for the DCAPP, which improves the control accuracy and control level of the DCAPP and is of great significance for realizing the accurate matching of load to power and operating speed to flow.

Although several research results have been achieved in this work, there are also some shortcomings. Affected by the flow leakage, the output flow and power values of the piston pump at this control method are smaller than the set values. Therefore, for further research, it will be our focus to add leakage flow compensation to the control method to achieve more accurate output control.

■ AUTHOR INFORMATION

Corresponding Author

   Qingliang Zeng − College of Mechanical and Electronic Engineering, Shandong University of Science and Technology, Qingdao 266590, China; College of Information Science and Engineering, Shandong Normal University, Jinan 250358, China; ⊙ orcid.org/0000-0002-3842-9107; Email: qlzeng@sdust.edu.cn

Authors

   Zhiyuan Sun − College of Mechanical and Electronic Engineering, Shandong University of Science and Technology, Qingdao 266590, China; ⊙ orcid.org/0000-0003-0557-6781

   Lirong Wan − College of Mechanical and Electronic Engineering, Shandong University of Science and Technology, Qingdao 266590, China

   Jinying Jiang − College of Mechanical and Electronic Engineering, Shandong University of Science and Technology, Qingdao 266590, China

Complete contact information is available at:
https://pubs.acs.org/10.1021/acsomega.3c03046

Notes

The authors declare no competing financial interest.

■ ACKNOWLEDGMENTS

■ NOMENCLATURE

A_d, A_x	action area of the large/small cavity of the actuator piston
$A_{pin,i}$, $A_{pout,i}$	flow area between the inlet/outlet silencing groove and the piston cavity
c_{ap}	viscous damping coefficient of the actuator piston
C_d	flow coefficient
C_l	internal leakage coefficient of the actuator piston
c_{sp}	damping coefficient of the swash plate
D	diameter of the piston pitch circle
DCAPP	double-compound axial piston pump
d_p	piston diameter
d_{tp}	diameter of the piston damping orifice
E	bulk modulus of the hydraulic oil
e_p	eccentricity between the piston and the piston cavity
$F_{p,i}$	equivalent force of oil pressure on the piston
$F_{pty,i}$, $F_{ptz,i}$	projections of the composite force $F_{pt,i}$ on the z-axis and y-axis
F_{sp}	force of the swash plate on the actuator piston
$F_{vlpc,i}$	viscous friction caused by leakage of the piston−cylinder block pair
$F_{vlsy,i}$, $F_{vlsz,i}$	projections of the composite force $F_{vls,i}$ on the z-axis and y-axis
h_p	diameter clearance between the piston and the piston cavity
h_{ppc}	clearance between the cylinder block and the port plate
h_{ssp}	clearance between the slipper and the swash plate
J_{sp}	rotational inertia of the swash plate
k_c	flow−pressure coefficient
k_p	displacement gradient of the piston pump
k_q	flow gain
l	lead
$l_{pc,i}$	contact length between the piston and the piston cavity
L_{sp}	acting force arm of the actuator piston to the swash plate
l_{tp}	length of the piston damping orifice
m_{ap}	mass of the actuator piston
N	number of pulses
p_{ap}	pressure of the large cavity of the actuator piston
p_c	pressure of the leakage cavity
p_d	outlet pressure of the pump
$p_{p,i}$	pressure of the piston cavity
p_s	inlet pressure of the pump
Q_l	total leakage flow
$Q_{lpcb,i}$	leakage flow between the piston and the cylinder block
Q_{lppc}	leakage flow between the port plate and the cylinder block
$Q_{lssp,i}$	leakage flow between the slipper and the swash plate
$Q_{pin,i}$, $Q_{pout,i}$	inlet/outlet flow of the piston cavity
R	radius of the piston pitch circle
r_{ext1}, r_{ext2}	inner/outer radius of the external port plate
r_{int1}, r_{int2}	outer/inner radius of the internal port plate
r_{spi}, r_{spo}	inner/outer radius of the slipper
r_{XY}	Pearson correlation coefficient
T_{sf}	shaft torque of the piston pump
T_{sp}	torque applied to the swash plate by the piston
T_{vlpp}	viscous friction torque between the port plate and the cylinder block
$u_{p,i}$	Couette effect of the piston velocity on the leakage flow
V_0	structure dead volume of the piston cavity
V_{ap}	volume of the large cavity of the actuator piston
$V_{p,i}$	volume of the piston cavity
ω	rotational speed of the shaft

w_{sv}	flow area of the servo valve
x_{ap}	displacement of the actuator piston
X_i, Y_i	data points
x_{sv}	displacement of the servo valve spool
$y_{p,i}$	force arm of the composite force along the z-axis in the y-direction
z	number of pistons
$z_{p,i}$	force arm of the composite force along the y-axis in the z-direction
β	inclination angle of the swash plate
β_0	initial inclination angle of the swash plate
$\theta_{in}, \theta_{out}$	angle range of the silencing groove at the inlet/ outlet of the port plate
θ_s	step angle
μ	dynamic viscosity
ρ	density of hydraulic oil

■ REFERENCES

(1) Wang, L. K.; Book, W. J.; Huggins, J. D. Application of Singular Perturbation Theory to Hydraulic Pump Controlled Systems. *IEEE-ASME Trans. Mechatron.* **2012**, *17*, 251−259.

(2) Lu, L.; Chen, Y.; Tong, C.; Ruan, J.; Li, S. Design strategy and performance evaluation of novel miniature two-dimensional (2D) piston pump with a dual stacking mechanism. *Alexandria Eng. J.* **2023**, *62*, 541−554.

(3) Zhao, J. A.; Fu, Y. L.; Ma, J. M.; Fu, J.; Chao, Q.; Wang, Y. Review of cylinder block/valve plate interface in axial piston pumps: Theoretical models, experimental investigations, and optimal design. *Chin. J. Aeronaut.* **2021**, *34*, 111−134.

(4) Manring, N.; Williamson, C. In *Calculating the Mechanical and Volumetric Efficiencies for Check-Valve Type, Digital Displacement Pumps*; BATH/ASME Symposium on Fluid Power and Motion Control; Univ Bath: Bath, England, Sep 12-14, 2018; Am. Soc. Mechanical Engineers: New York, 2018; pp 1−10 DOI: 10.1115/FPMC2018-8834.

(5) De Negri, V. J.; Wang, P.; Plummer, A.; Johnston, D. N. Behavioural prediction of hydraulic step-up switching converters. *Int. J. Fluid Power* **2014**, *15*, 1−9.

(6) Kogler, H. High dynamic digital control for a hydraulic cylinder drive. *Proc. Inst. Mech. Eng. Part I-J Syst Control Eng.* **2022**, *236*, 382−394.

(7) Tang, H. B.; Yang, W. X.; Wang, Z. C. A Model-Based Method for Leakage Detection of Piston Pump Under Variable Load Condition. *Ieee Access* **2019**, *7*, 99771−99781.

(8) Ying, P.; Tang, H.; Chen, L.; Ren, Y.; Kumar, A. Dynamic modeling and vibration characteristics of multibody system in axial piston pump. *Alexandria Eng. J.* **2023**, *62*, 523−540.

(9) Budden, J. J.; Williamson, C. *Danfoss Digital Displacement Excavator: Test Results and Analysis*, ASME/Bath Symposium on Fluid Power and Motion Control, Oct 7-9, 2019; Am. Soc. Mechanical Engineers: New York, Longboat Key: FL, USA, 2020; pp 1−10 DOI: 10.1115/FPMC2019-1669.

(10) Li, C. S.; Wang, X.; Qi, H. B.; Liu, X. Y.; Liu, X. H. Pressure performance improvement by dual-mode control in digital pump/motor. *J. Cent. South Univ.* **2020**, *27*, 2628−2642.

(11) Williamson, C.; Manring, N.; Asme, A. In *More Accurate Definition of Mechanical and Volumetric Efficiencies for Digital Displacement (R) Pumps*; Longboat Key: FL, USA, Oct 07-09, 2019; Am. Soc. Mechanical Engineers: New York, 2020; pp 1−11 DOI: 10.1115/FPMC2019-1668.

(12) Manring, N.; Williamson, C. The Theoretical Volumetric Displacement of a Check-Valve Type, Digital Displacement Pump. *J. Dyn. Syst., Meas., Control-Trans. ASME* **2019**, *141*, No. 031014.

(13) Heikkilä, M.; Linjama, M. Displacement control of a mobile crane using a digital hydraulic power management system. *Mechatronics* **2013**, *23*, 452−461.

(14) Spanu, A.; Alexandrescu, N. Mechatronic system used for flow controlling of hydraulic pumps with axial pistons. *UPB Sci. Bull., Series D: Mechan. Eng.* **2011**, *73*, 207−216.

(15) Heitzig, S.; Sgro, S.; Theissen, H. Energy efficiency of hydraulic systems with shared digital pumps. *Int. J. Fluid Power* **2012**, *13*, 49−57.

(16) Song, F.; Lou, J.; Peng, L. In *Energy-saving improvement and simulation study on digital hydraulic system*; International Conference on Advanced Mechatronic Systems, ICAMechS 2015, Beijing, China, Aug 22−24, IEEE Computer Society, 2015; Vol. 2015-October, pp 310−315. DOI: 10.1109/ICAMechS.2015.7287080.

(17) Wang, L.; Liu, X.-H.; Wang, X.; Chen, J.-S.; Liang, Y.-J. Shifting strategy of digital hydraulic transmission system for wheel loader. *Jilin Daxue Xuebao (Gongxueban)/J. Jilin Univer. (Eng. Technol. Ed.)* **2017**, *47*, 819−826.

(18) Gong, J.; Zhang, D. Q.; Guo, Y.; Liu, C. S.; Zhao, Y. M.; Hu, P.; Quan, W. C. Power control strategy and performance evaluation of a novel electro-hydraulic energy-saving system. *Appl. Energy* **2019**, *233−234*, 724−734.

(19) Mitov, A.; Kralev, J.; Slavov, T.; Angelov, I. In *Design of Embedded Control System for Open Circuit Axial Piston Pump*; 22nd International Symposium on Electrical Apparatus and Technologies, SIELA 2022, Bourgas, Bulgaria, June 1-4, Institute of Electrical and Electronics Engineers Inc., 2022; pp 1−4 DOI: 10.1109/SIELA54794.2022.9845787.

(20) Mitov, A.; Slavov, T.; Kralev, J. Rapid Prototyping of H∞ Algorithm for Real-Time Displacement Volume Control of Axial Piston Pumps. *Algorithms* **2023**, *16*, 120.

(21) Chao, Q.; Xu, Z.; Tao, J.; Liu, C. Capped piston: A promising design to reduce compressibility effects, pressure ripple and cavitation for high-speed and high-pressure axial piston pumps. *Alexandria Eng. J.* **2023**, *62*, 509−521.

(22) Zhao, K. P.; He, T.; Wang, C. L.; Chen, Q. M.; Li, Z. P. Lubrication characteristics analysis of slipper pair of digital valve distribution axial piston pump. *Adv. Mech. Eng.* **2022**, *14*, 168781322210854.

(23) Sun, Z. Y.; Zeng, Q. L.; Wan, L. R.; Dai, H. Z. Control and Dynamic Characteristics Analysis for the Double-Compound Axial Piston Pump Based on Working Conditions. *Machines* **2022**, *10*, No. 411.

(24) Edge, K. A.; Darling, J. The Pumping Dynamics of Swash Plate Piston Pumps. *J. Dyn. Syst., Meas., Control* **1989**, *111*, 307−312.

(25) Marinaro, G.; Frosina, E.; Senatore, A. A Numerical Analysis of an Innovative Flow Ripple Reduction Method for External Gear Pumps. *Energies* **2021**, *14*, No. 471.

(26) Bergada, J. M.; Kumar, S.; Davies, D. L.; Watton, J. A complete analysis of axial piston pump leakage and output flow ripples. *Appl. Math. Model.* **2012**, *36*, 1731−1751.

(27) Mandal, N. P.; Saha, R.; Sanyal, D. Theoretical simulation of ripples for different leading-side groove volumes on manifolds in fixed-displacement axial-piston pump. *Proc. Inst. Mech. Eng. Part I-J Syst. Control Eng.* **2008**, *222*, 557−570.

(28) Bergada, J. M.; Watton, J.; Kumar, S. Pressure, flow, force, and torque between the barrel and port plate in an axial piston pump. *J. Dyn. Syst., Meas., Control* **2008**, *130*, No. 011011.

(29) Imagine, S. A. *HYD Advanced Fluid Properties*; Technical Bulletin no. 117; Siements: Munich, Germany, 2007.